

## Synchrotron Radiation in the Study of Magnetism

D. B. McWhan

National Synchrotron Light Source, Brookhaven National Laboratory, Upton,  
NY 11973-5000, USA

(Received 2 May 1994; accepted 13 June 1994)

The use of synchrotron radiation in the study of magnetism is reviewed. An overview of resonant and non-resonant magnetic scattering is given along with their relation to well known magneto-optical effects such as magnetic linear and circular dichroism, Faraday rotation, and the magneto-optical Kerr effect. The use of these effects is reviewed for ferromagnetic iron, antiferromagnetic holmium and magnetic multilayers.

**Keywords:** magnetism; magneto-optical effects.

### Introduction

From the original compass to neodymium iron permanent magnets and magnetic storage media, the study of magnetism remains an active area of both pure and applied research. The field is expanding rapidly because of advances that have been made by materials scientists in synthesizing new materials atomic layer by atomic layer. The realization that X-rays could be used to probe the magnetic properties of materials coincided with the development of synchrotron sources, and most of the magneto-optical effects observed with visible light have been extended to the soft and hard X-ray region. In this article, the various types of scattering, absorption and photo-emission experiments are summarized and then illustrated for the elemental ferromagnet, Fe, and antiferromagnet, Ho. Finally, the importance of synchrotron radiation in the study of magnetic thin films is illustrated by a few examples. The field is expanding so rapidly that it is difficult to give a comprehensive review in the space allotted, and the examples are chosen to illustrate the range of applications rather than to be all inclusive.

### Theory

Magneto-optics refers to the change in the polarization of photons after transmission through or reflection from a magnetically ordered material. The most common effects are Faraday rotation, the magneto-optical Kerr effect and magnetic linear (MLD) or circular (MCD) dichroism. Faraday and Kerr rotation are the change in polarization on transmission through or reflection from a magnetic material, respectively, and dichroism is the difference in the absorption coefficient for  $\sigma$ - and  $\pi$ -polarized photons and circularly polarized photons with positive and negative helicity for MLD and MCD, respectively. These effects are defined in terms of changes in the real or the imaginary part of the index of refraction, and the real and imaginary parts are related to each other *via* the Kramers–Kronig transfor-

mation. Finally, the optical theorem relates the absorption coefficient to the imaginary part of the forward scattering amplitude (Jackson, 1975)

$$\mu = 2\lambda N \text{Im}[f(\mathbf{k}_f = \mathbf{k}_i, \mathbf{e}_f = \mathbf{e}_i)], \quad (1)$$

where  $N$  is the number of scatterers per unit volume, and  $\mathbf{k}_f$  and  $\mathbf{k}_i$  and  $\mathbf{e}_f$  and  $\mathbf{e}_i$  are the final and initial wavevectors and polarization vectors, respectively. Therefore, in principle, magneto-optics and scattering experiments are all inter-related, and the choice of experiment is governed by the type of information required. The early distinction between absorption experiments being used to obtain spectroscopic information on local magnetic properties, and scattering experiments being used for information on long-range magnetic order, is less sharply defined in resonant scattering experiments. As magneto-optical experiments are a special case of scattering experiments, the interaction of X-rays with magnetic materials will be summarized for the latter.

For simplicity the interaction of photons with the Fourier transforms of the spin,  $\mathbf{S}(\mathbf{K})$ , and orbital,  $\mathbf{L}(\mathbf{K})$ , angular momentum densities of a magnetic material is divided into two regimes depending on the energy of the incident photon. At high energies, which are far away from characteristic atomic energies, the weak direct interaction between the magnetic field of the photon and  $\mathbf{L}(\mathbf{K})$  and  $\mathbf{S}(\mathbf{K})$  is the leading term. This is a relativistic effect but can be visualized in a classical description as the electric or magnetic field of the photon accelerating the electron or its magnetic moment, which in turn reradiates as electric or magnetic dipole or quadrupole radiation (de Bergevin & Brunel, 1981). At lower energies the interaction is dominated by resonant terms which result from the promotion of inner-shell electrons to empty states above the Fermi surface. Strictly speaking these resonances are electric multipole transitions, and the sensitivity to magnetism results from lifting degeneracies of various energy levels by the spin-orbit and exchange interactions. This in turn affects the probability of the transitions that are allowed by the appro-

priate selection rules (Hannon, Trammell, Blume & Gibbs, 1988, 1989).

Following the initial suggestion by Platzman & Tzoar (1970) that X-rays could be used to determine magnetic structures, de Bergevin & Brunel (1972, 1981) gave a full theoretical description and demonstrated many of the important effects using conventional laboratory X-ray sources. Following Blume (1985) and Blume & Gibbs (1988), the magnetic contribution to the atomic scattering factor is given by:

$$f(\mathbf{K})^{\text{mag}} = ir_0 \frac{\hbar K}{mc} \left[ \frac{1}{2} \mathbf{A} \cdot \mathbf{L}_j(\mathbf{K}) + \mathbf{B} \cdot \mathbf{S}_j(\mathbf{K}) \right] \quad (2)$$

where  $r_0$  is the electron radius,  $\mathbf{K} = \mathbf{k}_i - \mathbf{k}_f$  is the momentum transfer, and  $\mathbf{A}$  and  $\mathbf{B}$  are complex matrices which depend on the wavevector and on the polarization of the incident and scattered photons. This magnetic scattering is much weaker than normal charge scattering because of the factor  $\hbar K/mc$ , which is typically  $\sim 0.01$ . Because the contributions of the orbital and spin terms to the scattering amplitude depend differently on the polarization, it is possible to separate them experimentally if the scattering geometry is chosen appropriately and if the polarization of the incident and scattered photons is determined as demonstrated for the case of antiferromagnetic holmium metal by Gibbs *et al.* (1988). The polarization dependences of normal charge scattering ( $\mathbf{e}^* \cdot \mathbf{e}$ ) and magnetic scattering are also fundamentally different and thus the two can be distinguished by using polarized X-ray scattering experiments.

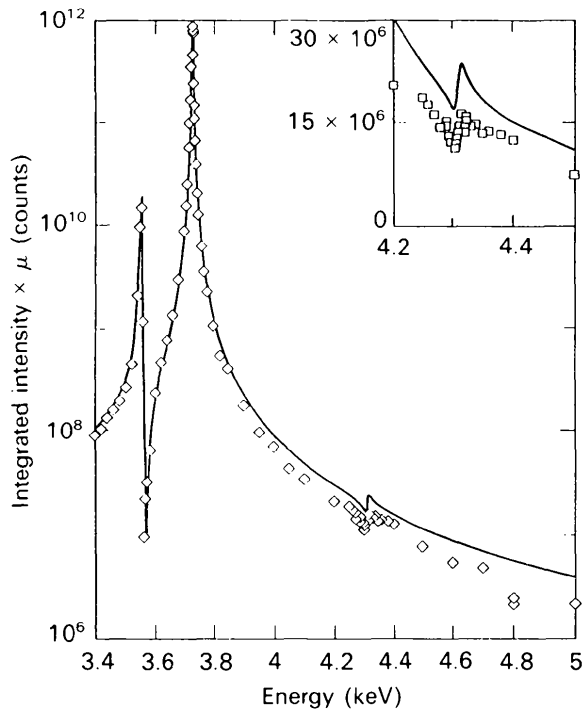


**Figure 1**  
Intensity of antiferromagnetic reflections in UAs versus photon energy showing the X-ray magnetic resonant scattering at the  $M_5$ ,  $M_4$  and  $M_3$  absorption edges. The solid curve is the coherent sum of three dipole oscillators (McWhan *et al.*, 1990).

X-ray resonant-exchange scattering was first observed in ferromagnetic nickel by Namikawa, Ando, Nakajima & Kawata (1985) and in antiferromagnetic holmium by Gibbs *et al.* (1988, 1991). The theory has been developed by Hannon *et al.* (1988, 1989) for both dipole and quadrupole transition, and extended by Luo, Trammell & Hannon (1993) in the fast-collision approximation for elastic and inelastic resonant X-ray scattering. The atomic scattering amplitude for the dipole approximation is given by:

$$f_{\text{res}}^{\text{mag}} = (3\lambda/8\pi) \{ \mathbf{e}_f^* \cdot \mathbf{e}_i [F_{11} + F_{1-1}] - i(\mathbf{e}_f^* \times \mathbf{e}_i) \cdot \mathbf{z}_j [F_{11} - F_{1-1}] + (\mathbf{e}_f^* \cdot \mathbf{z}_j)(\mathbf{e}_i \cdot \mathbf{z}_j) [2F_{10} - F_{11} - F_{1-1}] \}. \quad (3)$$

where  $\mathbf{e}_f^*$  and  $\mathbf{e}_i$  are the polarization of the final and incident photons, and  $\mathbf{z}_j$  is the magnetization direction of the atomic magnetic moment. The terms  $F_{LM}$ , where  $L$  is the order of the transition ( $L = 1$  for dipole transitions) and  $M$  is

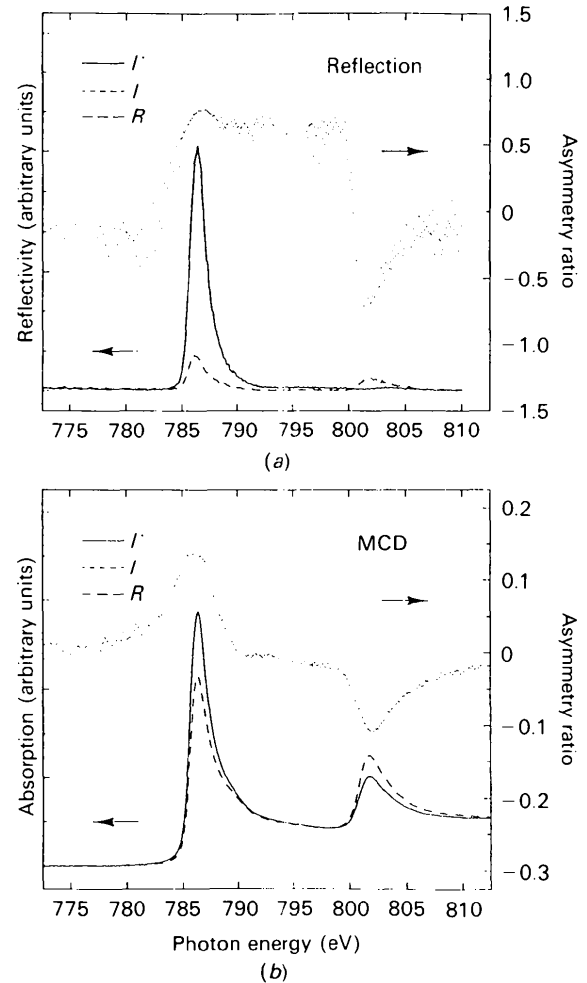


**Figure 2**  
(a) Two circularly polarized reflectivity curves from a thin Co film at the  $L_3$  and  $L_2$  absorption edges. The experimental configuration is that of the longitudinal magneto-optical Kerr effect with an incident angle of  $25^\circ$  and a measurement angle of  $45^\circ$ . (b) The corresponding magnetic circular dichroism (Kao *et al.*, 1994).

the change in angular momentum ( $\Delta M = 0, \pm 1$ ), are composed of matrix elements which couple the ground and excited states *via* the dipole operator, the probabilities that the ground state is occupied and that the excited state is empty, and a resonant-energy denominator. The resonant-scattering amplitude contains three terms, each of which has a different polarization dependence. The first is independent of the direction of the magnetic moment, and it leads to the usual anomalous-scattering corrections to the charge scattering. The second term is linear in the magnetic moment direction. In an antiferromagnet this term produces reflections in reciprocal space at the wavevector of the magnetic structure, and in a ferromagnet gives magnetic contributions to the charge reflections. In the latter case, these contributions can be measured by reversing the direction of the magnetic moment with an external magnetic field or reversing the helicity of circularly polarized X-rays. The third term is quadratic in the moment direction. For the case of forward scattering, the second and third terms lead to magnetic circular and linear dichroism, respectively (Carra & Altarelli, 1990).

The resonant terms originate in the transitions of core electrons to empty excited states above the Fermi level, and the resonant energy of each transition is specific to the element and even to the chemical environment of the element. This provides a unique probe of magnetic materials. The spin polarization of the density of empty states can be mapped out as a function of energy and also by symmetry of the electronic bands. The dipole selection rules govern which states are probed. The  $K$  absorption edge couples  $s$  core states to  $p$  bands; the  $L_2$  and  $L_3$  edges of transition metals and rare-earth metals couple spin-orbit-split  $p$  states

to  $d$  bands, and the  $M_4$  and  $M_5$  edges of actinide metals couple  $d$  core states to the  $5f$  bands. In many rare-earth metals quadrupole transitions are observed which couple core  $p$  states to  $4f$  bands. The resonant effects at  $M$ ,  $L$  and  $K$  absorption edges are illustrated in Figs. 1, 2 and 3. In Fig. 1, the intensity of an antiferromagnetic reflection in uranium arsenide is plotted as a function of energy through several of the uranium  $M$  absorption edges (McWhan *et al.*, 1990). The maximum intensity is 1% of a typical charge reflection, and the data are well fitted by the functional form expected for the coherent sum of three dipole oscillators. In Fig. 2, the longitudinal magneto-optical Kerr effect and the magnetic circular dichroism in ferromagnetic cobalt are plotted as a function of energy through the  $L_3$  and  $L_2$  absorption edges (Kao *et al.*, 1994). The asymmetry ratio approaches 80% at some energies. In Fig. 3, the asymmetry ratio for magnetic circular dichroism and the Kramers–Kronig transform of Faraday rotation measurements on ferromagnetic Fe are plotted *versus* energy through the  $K$  absorption edge (Maruyama *et al.*, 1991; Hart, Siddons & Stajanoff, 1991).

An antiferromagnet like UAs can be studied using linearly polarized X-rays. For an incident beam with  $\sigma$  polarization it can be seen from (3) that the scattered beam has  $\pi$  polarization. The rotation of the linear polarization is measured directly in the Faraday effect whose Kramers–Kronig transform is shown in Fig. 3. The magneto-optical Kerr effect and magnetic circular dichroism involve the difference in scattering amplitude or absorption of circularly polarized X-rays with positive and negative helicity. There are different conventions in use in the definition of circular polarization and of the reference direction

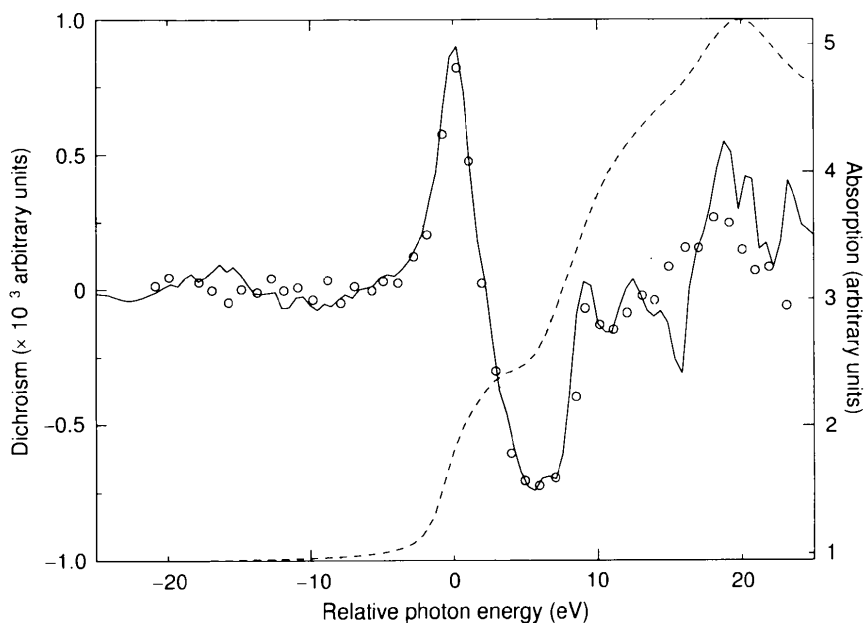


**Figure 3**

Comparison of magnetic circular dichroism (open circles) and Kramers–Kronig transformation of Faraday effect measurement (solid line) in Fe at the  $K$  absorption edge. The dashed and dotted lines are the absorption measurements taken in conjunction with the MCD and Faraday experiments of Maruyama *et al.* (1991) and Hart *et al.* (1991), respectively.

of the sample, and both appear in the recent literature. For a photon propagating in the  $z$  direction, a circularly polarized beam with positive helicity is defined as  $\mathbf{e}_x + i\mathbf{e}_y$ . This beam has a positive projection of the angular momentum along  $z$  (Jackson, 1975), and in an absorption experiment with the spin of the majority electrons parallel to  $z$ , dipole selection rules favor transitions from the  $2p_{3/2}$  to the majority spin band at the  $L_3$  edge and from the  $2p_{1/2}$  to the minority spin band at the  $L_2$  edge. The sign of the asymmetry ratio at each edge gives direct spectroscopic information about the majority and minority spin density of states above the Fermi level. In Fig. 2, the asymmetry ratio is defined as  $R = (I^+ - I^-)/(I^+ + I^-)$  where  $I^+$  is defined as the applied magnetic field being parallel to the photon spin and therefore, antiparallel to the direction of the spin of the majority electrons. In this case, a positive MCD signal at the  $L_3$  edge implies a larger density of unoccupied minority spin states. By contrast, the convention used in Fig. 3 (Hart *et al.*, 1991; Maruyama *et al.*, 1991) defines  $I^+$  as the spin of the majority electrons parallel to the photon spin and would give the opposite sign of the MCD signal at the  $L_3$  edge of Co. Note that resonances at the  $L$  edge couple to  $3d$  states (Fig. 2) and at the  $K$  edge to  $4p$  states (Fig. 3), so that depending on the details of the band structure, the MCD signals may have the same or opposite signs. There is a tendency for spectroscopists to use the convention in Fig. 3 where the reference direction is the spin direction of the majority electrons as opposed to the applied magnetic field commonly used in flipping ratio measurements.

Unlike pure magnetic scattering,  $\mathbf{L}(\mathbf{K})$  and  $\mathbf{S}(\mathbf{K})$  cannot be separated in resonant-scattering experiments. However, for forward scattering, approximate sum rules have been derived for the integral of the imaginary part of  $f_{\text{res}}^{\text{mag}}$  over two spin-orbit-split absorption edges,  $j_+$  and  $j_-$  (Thole, Carra, Sette & van der Laan, 1992; Carra, Thole, Altarelli & Wang, 1993). The sum rules are given in terms of the absorption coefficients for circular polarization with positive and negative helicity by:

$$\frac{\int_{j_+, j_-} d\omega(\mu^+ - \mu^-)}{\int_{j_+, j_-} d\omega(\mu^+ + \mu^- + \mu^0)} \simeq (1/2)C_{cln}\langle L_z(0) \rangle \quad (4)$$

$$\frac{\int_{j_-} d\omega(\mu^+ - \mu^-) - [(c+1)/c]\int_{j_+} d\omega(\mu^+ - \mu^-)}{\int_{j_+, j_-} d\omega(\mu^+ + \mu^- + \mu^0)} \simeq D_{lcn}\langle S_z(0) \rangle + E_{lcn}\langle T_z \rangle \quad (5)$$

where  $C_{cln}$ ,  $D_{lcn}$  and  $E_{lcn}$ , are coefficients defined in terms of  $c$  and  $l$  which are the quantum numbers for the core and excited states, respectively, and  $n$ , which is the number of electrons in the ground state  $I^n$  configuration.  $L_z(0)$  and  $S_z(0)$  are the ground-state expectation values for the orbital and spin angular momentum densities and  $T_z$  is a magnetic dipole term. The integral of the MCD signals from each of the two spin-orbit-split resonances would cancel if there was no orbital moment (4), and the asymmetry of the integrals is a direct indication of the orbital moment. Similarly, if  $T_z$  can be calculated, then  $\langle S_z(0) \rangle$  can be obtained from

(5). For example, integrating the MCD signal shown in Fig. 2 gives an orbital moment of  $0.14 \mu_B$  and a spin moment of  $1.52 \mu_B$  (Chen *et al.*, 1994;  $1 \mu_B = 9.274078 \times 10^{-24} \text{ J T}^{-1}$ ). These are in agreement with the values obtained from Einstein-de Haas gyromagnetic ratios of 0.15 and 1.52 (Scott & Sturmer, 1969; Reck & Fry, 1969). Measurements of the magnetic form factor by polarized neutron scattering are in agreement with a model of a total spin moment of  $1.58 \mu_B$  and an orbital moment of  $0.13 \mu_B$  (Moon, 1964). However, in this model the ratio of the orbital to spin moment was taken from the gyromagnetic ratio measurements and is not an independent determination. In modeling the neutron data, the spin component was divided into a  $3d$  and conduction  $s$  electron components. As the dipole selection rules allow transitions from the  $p$  core levels to both components, the MCD measurements should sample the total spin moment. Detailed band-structure calculations are consistent with the orbital sum rule (Wu, Wang & Freeman, 1993); but the spin sum rule may be less accurate (Wu, Stöhr, Hermsmeier, Samant & Weller, 1992).

### Ferromagnetic iron

The first property of interest is the magnetic structure. In their demonstration experiment de Bergevin & Brunel (1981) measured small changes in the intensity of the (110) and (211) Bragg reflections when the magnetization direction was reversed with an external magnetic field. They compared the changes in intensity with values calculated from the known magnetic structure of iron. The observed and calculated values for the flipping ratios were:  $(\Delta I/I) \times 10^3 = 0.42$  and  $0.36$  (110);  $0.42$  and  $0.38$  (211). By varying the scattering geometry and the polarization of the incident beam it would be possible to measure the magnetic scattering from a set of Bragg reflections and then to determine the magnetic structure of a new magnetic material. As in the case of neutron scattering, the intensity of the magnetic component (2) can be put on an absolute scale by comparison with the known charge scattering. Consequently,  $\mathbf{L}(\mathbf{K})$  and  $\mathbf{S}(\mathbf{K})$  can be determined directly. For a circularly polarized white beam incident on a sample with the moment aligned either parallel to the incident or to the scattered beam,  $\mathbf{L}(\mathbf{K})$  or  $\mathbf{L}(\mathbf{K}) + \mathbf{S}(\mathbf{K})$  can be measured, respectively (Collins, Laundy & Rollason, 1992). In this energy-dispersive technique the  $\mathbf{K}$  dependence of the respective components,  $\mathbf{L}(\mathbf{K})$  and  $\mathbf{S}(\mathbf{K})$ , of the magnetic form factor can be measured in a single experiment. This cannot be achieved by any other technique. The results for Fe are in agreement with the calculated form factor of Fe and that derived by modeling the neutron scattering results (Collins *et al.*, 1992; Fisher *et al.*, 1993).

Turning to the determination of  $\mathbf{L}(0)$  and  $\mathbf{S}(0)$  using magnetic circular dichroism and the sum rules at the  $L_2$  and  $L_3$  edges, the most recent measurements on Fe by Chen *et al.* (1994) give  $\mu_{\text{orb}} = 0.090 \mu_B$  and  $\mu_{\text{spin}} = 2.21 \mu_B$ . These values are to be compared with those obtained from measurements of the gyromagnetic ratio of 0.092 and 2.08

(Scott & Sturmer, 1969; Reck & Fry, 1969). These measurements are a stringent test of recent band-structure calculations which give 0.090 and 2.21 (Söderlind, Eriksson, Johansson, Albers & Boring, 1992) and 0.05 and 2.16 (Wu *et al.*, 1993). The resonances at the  $L$  edges can also be observed in a scattering experiment using linearly  $\pi$ -polarized X-rays and reversing the moment direction with an external magnetic field (Kao *et al.*, 1990). The reflectivity as a function of energy cannot be fitted simply by the coherent sum of two interfering dipole oscillators and, as also evident in the MCD measurements, additional structure can be seen in the resonance.

There is spectroscopic information in the structure of the resonances which is related to the density of unoccupied states above the Fermi level in the majority and minority spin bands. Fig. 3 shows MCD measurements as a function of energy through the  $K$  absorption edge of iron by Maruyama *et al.* (1991), along with the Kramers–Kronig transformation (solid curve) of Faraday rotation measurements on Fe by Hart *et al.* (1991) (see McWhan, Hastings, Kao & Siddons, 1992). There is good agreement between the two different measurements. The dominant features in the MCD data are a peak just above the Fermi level followed by a change in sign and a valley around 6–7 eV above the Fermi level. At the  $K$  absorption edge the relevant allowed dipole transitions are from  $1s$  core levels to unoccupied  $p_{1/2}$  or  $p_{3/2}$  states above the Fermi level. It is assumed that the  $p$  states are polarized by the unfilled  $d$  states, and the peak and the valley in the MCD data are attributed to Fe having unoccupied  $p$  states in the majority and minority spin bands, respectively (Schütz *et al.*, 1987; Ebert, Strange & Gyorffy, 1988; Maruyama *et al.*, 1991). By contrast Ni has a single large valley in the MCD data reflecting the unoccupied minority spin states above the Fermi level (Maruyama *et al.*, 1991).

Spectroscopic information about the polarization of the core levels can be obtained from  $2p$  and  $3p$  core-level photoemission experiments on Fe. In a photoemission experiment the electron is raised to energies far above the Fermi level where there is no structure in the final state, and the observation of dichroism requires that the core levels be split by spin-orbit or exchange interactions. Baumgarten, Schneider, Petersen, Schäfers & Kirschner (1990) measured the  $2p_{1/2}$  and  $2p_{3/2}$  photoemission using circularly polarized X-rays with positive and negative helicity and also reversing the moment direction with a field. They observed an exchange splitting of 0.3 (2) and 0.5 (2) eV for the  $2p_{1/2}$  and  $2p_{3/2}$  spin-orbit-split core levels, respectively. More recently, linear magnetic dichroism has been observed in angular resolved photoemission from Fe  $3p$  core levels (Roth, Hillebrecht, Rose & Kisker, 1993). For  $\pi$ -polarized X-rays, the spin-resolved majority and minority resonances show structure in the spectra which is attributed to a spin-orbit splitting of the  $3p_{1/2}$  and  $3p_{3/2}$  levels of 0.7 eV.

Moving up to the valence bands, spin-resolved resonant photoemission studies provide insight into itinerant mag-

netism in the transition metals. Kisker, Schröder, Campagna & Gudat (1984) observed almost no temperature dependence in the energy of the exchange-split majority and minority spin states near the Curie temperature, but the intensity of the resonance decreased with increasing temperature. In the Stoner model, the exchange splitting decreases to zero with increasing temperature at the Curie temperature, and Haines, Clauberg & Feder (1985) showed that a model incorporating short-range magnetic order can account for the observed spin-resolved photoemission data. Further evidence for a fluctuating local magnetic moment model of itinerant ferromagnetism has been given by recent measurements on Ni by Kakizaki *et al.* (1994).

Photoemission is a surface-sensitive probe, and it has been used to address the question of whether the surface layer of iron is paramagnetic or ferromagnetic and whether the moment at the surface is enhanced. Brookes, Clarke, Johnson & Weinert (1990), observed magnetic surface states in Fe(001) using spin-polarized angle-resolved photoemission and measured binding energies for the magnetic surface state which are consistent with 7- and 13-layer full-potential linearized-augmented plane-wave calculations. These calculations predicted enhanced magnetic moments in the surface region. Evidence for this enhancement was obtained from  $3p$  spin-polarized photoemission experiments on iron films grown epitaxially onto W(110) (Mulhollan, Andrews & Erskine, 1992). Bulk-like magnetic order was observed in a film which was 1.5 monolayers thick, and the core-level exchange splitting decreased 60% on doubling the thickness of the Fe films.

In summary, synchrotron radiation experiments on Fe yield magnetically sensitive information ranging from the structure, magnetic moment, form factor, Fourier transform of both the orbital and spin angular momentum densities, spectroscopic information about the polarization of the empty states above the Fermi surface, and both the spin-orbit and the exchange splitting of core levels. The results of these experiments provide critical tests of theories of itinerant magnetism and the evolution of magnetic order at surfaces and in thin films.

### Antiferromagnetic holmium

Holmium metal has been studied extensively using magnetic X-ray scattering because of its large magnetic moment ( $10.6 \mu_B$ ). Holmium orders in a spiral structure in which the moments in each layer of the hexagonal close-packed structure are aligned ferromagnetically and the moment direction in each layer was thought to rotate by an angle  $\alpha$  with respect to the adjacent layer. The structure is incommensurate in that  $\alpha$  is not a simple fraction of  $360^\circ$ . High-resolution magnetic X-ray scattering measurements revealed that  $\alpha$  is not a smoothly varying function of temperature as had been concluded from earlier neutron scattering studies (Gibbs, Moncton, D'Amico, Bohr & Grier, 1985; Bohr, Gibbs, Moncton & D'Amico, 1986). There are ranges of temperature in which phases with simple frac-

tions such as 5/27, 2/11, or 2/12 exist. Moreover, in addition to the magnetic Bragg reflections resulting from the spiral structure, additional reflections were found at some temperatures. These were shown to be charge as opposed to magnetic reflections by analyzing their polarization dependence. A new model for the magnetic structure was developed as a result of these studies in which pairs of ferromagnetically aligned layers rotate together. In order to come close to commensurability there are periodic spin slips where a single layer, as opposed to pairs of layers, appears in the stacking sequence. These result in a new periodicity which accounts for the appearance of the charge reflections. On the basis of the Ho results, the other heavy rare-earth metals were re-examined by magnetic X-ray scattering and neutron scattering and the spin-slip model was found to be applicable to the whole series. A theory for the rare-earth magnetic structures has been developed which accounts for these observations (Mackintosh & Jensen, 1991). The intrinsic high resolution, and the ability to distinguish between magnetic and charge scattering in X-ray studies, provides a powerful tool in the determination of magnetic structures.

Although not directly magnetic scattering, an anisotropy develops in the atomic scattering factor of holmium when it orders, because the partially filled  $4f$  orbitals do not have spherical symmetry. When the moments become aligned below the Néel temperature a charge peak develops at a wavevector that is twice the magnetic peak. This effect was first observed in Ho by Keating (1969).

The first demonstration of the separation of  $L(\mathbf{K})$  and  $S(\mathbf{K})$  using magnetic X-ray scattering techniques was performed on Ho (Gibbs *et al.*, 1988). Using an incident beam with  $\sigma$  polarization, the  $\sigma$  and  $\pi$  components of the scattered beam were measured for the magnetic reflections around the (002), (004) and (006) Bragg reflections. The wavevector dependencies of the orbital and spin contributions to the magnetic scattering given by (2) were observed. It had been hoped that the subtle differences in the wavevector dependencies of the spin and orbital magnetic form factors could be measured, but the limited accuracy of the first experiments obscured the differences.

The theory for X-ray resonant-exchange scattering was developed to understand the observations made on Ho (Hannon *et al.*, 1988). A large resonant enhancement was observed in the intensity of the magnetic reflection as the energy of the incident X-ray beam was tuned through the  $L_3$  absorption edge (Gibbs *et al.*, 1988). For a spiral magnetic structure the magnetic reflections occur as satellites around the Bragg reflections for the hexagonal close-packed structure, and in addition to the first-order satellites, second-, third- and fourth-order satellites were observed on resonance in Ho in the antiferromagnetic phase. It was also apparent that instead of a single resonance as a function of energy there were two resonances, and each satellite and resonance had a different polarization dependence. The model of Hannon *et al.* (1988) identified the resonances as magnetic sensitive electric dipole and quadrupole transi-

tions from core levels to unoccupied states above the Fermi level, and it predicted both the higher order satellites and their polarization dependence. The dipole transitions led to only first- and second-order satellites in which the polarization of the incident and scattered beams were  $\sigma - \pi$  and  $\sigma - \sigma$ , respectively. Similarly, four satellites with a more complicated polarization dependence occur for quadrupole transitions. In absorption spectroscopy pre-edge features are often observed and attributed to quadrupole transitions, but attempts to verify this agreement on the basis of the predicted angular dependence of the absorption coefficient have not been successful. The observation of four satellites with the predicted polarization dependence clearly establishes the quadrupole nature of the pre-edge resonance.

The enhancement of the intensity on resonance makes it feasible to study weak effects such as critical scattering above the Néel temperature and surface-sensitive effects. The evolution of coherent fluctuations as the temperature approaches the Néel temperature provides an important test of the theory of second-order phase transitions. The average size of the fluctuating domains diverges as a power of the reduced temperature which depends on the universality class of the transition. In Ho within about 2 K of  $T_N$  two length scales were observed instead of the normal single length scale (Thurston *et al.*, 1993). This may reflect the surface sensitivity of X-ray scattering and reflect a strain-induced ordering in the near-surface region, which is different from that in the bulk.

In summary, recent X-ray studies on Ho have led to a new understanding of the incommensurate magnetic structures in the rare-earth metals and demonstrated the possibility of separating the orbital and spin angular momentum densities *via* X-ray scattering. Resonant scattering provides an important spectroscopic tool both to identify the origin of near-edge features and to study weak effects such as critical scattering.

### Magnetic thin films and multilayers

The use of synchrotron radiation to study magnetism coincided with the development of techniques to grow thin films and multilayers atomic layer by atomic layer, and synchrotron studies have played a major role in understanding these new materials. A number of different multilayer systems composed of alternating regions of magnetic and non-magnetic materials have been grown, and questions about (a) the magnetic structure within a given magnetic region, (b) the relative orientation of the moments in adjacent magnetic regions and (c) the polarization of the non-magnetic regions have been addressed using synchrotron radiation.

Gd-Y superlattices were one of the first to be studied in detail. Magnetization studies of single-crystal samples of  $Gd_n Y_m$  were found to show a reduced average magnetic moment, and a crystal of  $[Gd_{21} Y_{21}] \times 40$  (*i.e.* a sequence of 21 layers of Gd followed by 21 layers of Y repeated 40 times) was studied by non-resonant magnetic scattering

(Vettier *et al.*, 1986). The magnetic contributions to 20 reflections from the superlattice were derived from flipping ratios. The measurements were consistent with a simple ferromagnetic arrangement of the Gd moments in each layer with the reduced average moment per Gd resulting from a smooth decrease in the projected moment on going from the center of a Gd region toward the interfaces. In addition, the temperature dependence of the interplanar-spacing modulation in the superlattice, derived from the X-ray measurements, exhibited a large magnetostrictive component below the ordering temperature, which was consistent with the reduced moment in the interfacial region. Subsequent neutron scattering studies on a series of Gd–Y superlattices showed that adjacent blocks of Gd layers were aligned either ferromagnetically or antiferromagnetically depending on the number of intervening Y layers,  $m$ , and that there was an oscillatory dependence on  $m$  (Majkrzak *et al.*, 1986). The oscillatory behaviour is consistent with the coupling between Gd layers being *via* the Ruderman–Kittel–Kasuya–Yosida interaction (Yafet, 1987). Subsequently, a similar oscillatory dependence has been found in a number of magnetic multilayer systems by neutron scattering, but it is only recently that the anti- and ferromagnetic alignments have been studied in detail using resonant magnetic scattering at the Ni  $L_3$  edge in Ag–Ni multilayers (Tonnerre *et al.*, 1993).

The element and site specificity of resonant scattering and absorption measurements provide a powerful probe of magnetic structures. For example, Idzerda *et al.* (1993) have studied the growth of a trilayer structure of Fe–Cr–Fe using MCD. The relative orientation of the ferromagnetic moments can be obtained from the sign of the asymmetry ratio at the  $L_2$  and  $L_3$  edges of transition metals. A comparison of MCD measurements at the Fe and Cr edges shows that the first layer of Cr grown on Fe is aligned antiferromagnetically with respect to the Fe, but that a layer of Fe grown on top of the Cr is aligned antiferromagnetically with respect to the original Fe layer. In this way the growth of a magnetic multilayer structure can be studied layer by layer. A second example is the determination of element-specific magnetic hysteresis in a heteromagnetic multilayer. Bulk magnetization measurements as a function of magnetic field often yield complicated hysteresis loops. Chen *et al.* (1993) measured the hysteresis loop *via* MCD as a function of magnetic field in a trilayer structure composed of layers of Fe/Cu/Co. The hysteresis loop derived from MCD at the Fe  $L_3$  edge was square and sharp while that from the Co  $L_3$  edge was rounded and broad.

In a multilayer composed of alternating regions of magnetic and non-magnetic components there are questions about the moment distribution near the interfaces and about the coupling mechanism between adjacent magnetic regions. In the rare-earth multilayers it is natural to assume that the coupling and the oscillatory behaviour discussed above result from the RKKY interaction. In transition-metal multilayers, the finite thickness of the magnetic regions is thought to lead to a quantization of the bulk band

structure perpendicular to the film, and the quantum-well states cross the Fermi level periodically as a function of film thickness. In order to address these questions, advantage is taken of the element-specific nature of resonant MCD and spin-polarized photoemission. Garrison, Chang & Johnson (1993) and Carbone, Vescovo, Rader, Gudat & Eberhardt (1993) used the latter technique to study thin films of copper deposited on Co(001). Both observed and characterized the quantum-well states, and the latter observed the oscillatory behavior in the intensity and in the spectral polarization at the Fermi level as a function of the thickness of the Cu layer. MCD measurements were used by Samant *et al.* (1994) to demonstrate an induced magnetic moment in the  $d$  shell of the Cu atoms of Co/Cu multilayers, and the results suggest that the polarization is largest near the interfaces of the Co regions. Similar results were found for Co/Pt multilayers by Schütz, Stähler, Knülle & Fischer (1993). Finally, studies of Co/Pd multilayers by Wu *et al.* (1992) demonstrated the enhancement of the Co moment over that observed in bulk Co, in agreement with recent theoretical predictions.

Combining the element specificity of MCD with soft X-ray microscopy, it is possible to image magnetic domains. Stöhr *et al.* (1993) have recorded images of magnetic bits on a CoPtCr magnetic recording disk with a lateral resolution of 1  $\mu\text{m}$  using MCD at the Co  $L_3$  and  $L_3$  edges. X-ray studies map nicely onto the needs of materials scientists to characterize magnetic thin films as demonstrated by these few examples. Measurements have covered the whole range of problems from structure to electronic properties to the macroscopic structure of magnetic domains.

## Summary

In this review, the different ways in which synchrotron radiation can be used to study magnetism have been summarized and examples given for a ferromagnetic metal, Fe, an antiferromagnetic metal, Ho, and for magnetic multilayers. These examples represent only a small subset of experiments in this rapidly growing field. Some other areas include studies of the evolution of magnetic order in random alloys such as  $\text{Mn}_{1-x}\text{Zn}_x\text{F}_2$  (Hill, Feng, Birgeneau & Thurston, 1993), heavy fermion superconductors such as  $\text{URu}_2\text{Si}_2$  (Isaacs *et al.*, 1990), small crystals of exotic materials such as NpAs (Langridge *et al.*, 1994) and mixed-valence materials such as TmSe (McWhan *et al.*, 1993). Other reviews of studies of magnetism using synchrotron radiation include Vettier (1994) and Lovesey (1993). In particular, magnetic Compton scattering, which is not discussed in this article, has been reviewed by Cooper (1985).

I thank C. T. Chen, P. D. Johnson and C.-C. Kao for many helpful discussions. This work was supported by the US Department of Energy Contract No. DE-AC02-76CH00016.

## References

- Baumgarten, L., Schneider, C. M., Petersen, H., Schäfers, F. & Kirschner, J. (1990). *Phys. Rev. Lett.* **65**, 492–495.
- Bergevin, F. de & Brunel, M. (1972). *Phys. Lett. A*, **39**, 141–142.
- Bergevin, F. de & Brunel, M. (1981). *Acta Cryst.* **A37**, 314–324.
- Blume, M. (1985). *J. Appl. Phys.* **57**, 3615–3618.
- Blume, M. & Gibbs, D. (1988). *Phys. Rev. B*, **37**, 1779–1789.
- Bohr, J., Gibbs, D., Moncton, D. E. & D'Amico, K. L. (1986). *Physica A*, **140**, 349–352.
- Brookes, N. B., Clarke, A., Johnson, P. D. & Weinert, M. (1990). *Phys. Rev. B*, **41**, 2643–2645.
- Carbone, C., Vescovo, E., Rader, O., Gudat, W. & Eberhardt, W. (1993). *Phys. Rev. Lett.* **71**, 2805–2808.
- Carra, P. & Altarelli, M. (1990). *Phys. Rev. Lett.* **64**, 1286–1288.
- Carra, P., Thole, B. T., Altarelli, M. & Wang, X. (1993). *Phys. Rev. Lett.* **70**, 694–697.
- Chen, C. T., Idzerda, Y. U., Lin, H.-J., Meigs, G., Chaiken, A., Prinz, G. A. & Ho, G. H. (1993). *Phys. Rev. B*, **48**, 642–645.
- Chen, C. T., Lin, H.-J., Meigs, G., Pellegrin, E., Smith, N. V., Idzerda, Y. U. & Ho, G. H. (1994). *Bull. Am. Phys. Soc.* **39**, 92.
- Collins, S. P., Laundry, D. & Rollason, A. J. (1992). *Philos. Mag. B*, **65**, 37–46.
- Cooper, M. J. (1985). *Rep. Prog. Phys.* **48**, 415–481.
- Ebert, H., Strange, P. & Gyorfyy, B. L. (1988). *J. Appl. Phys.* **63**, 3055–3057.
- Fisher, P., Schütz, G., Kaiser, W., Hunecke, J., Knülle, M. & Stähler, S. (1993). *J. Appl. Phys.* **73**, 5346.
- Garrison, K., Chang, Y. & Johnson, P. D. (1993). *Phys. Rev. Lett.* **71**, 2801–2804.
- Gibbs, D., Grübel, G., Harshman, D. R., Isaacs, E. D., McWhan, D. B., Mills, D. & Vettier, C. (1991). *Phys. Rev.* **43**, 5663–5681.
- Gibbs, D., Harshman, D. R., Isaacs, E. D., McWhan, D. B., Mills, D. & Vettier, C. (1988). *Phys. Rev. Lett.* **61**, 1241–1244.
- Gibbs, D., Moncton, D. E., D'Amico, K. L., Bohr, J. & Grier, B. (1985). *Phys. Rev. Lett.* **55**, 234–237.
- Haines, E. M., Clauberg, R. & Feder, R. (1985). *Phys. Rev. Lett.* **54**, 932–934.
- Hannon, J. P., Trammell, G. T., Blume, M. & Gibbs, D. (1988). *Phys. Rev. Lett.* **61**, 1245–1248.
- Hannon, J. P., Trammell, G. T., Blume, M. & Gibbs, D. (1989). *Phys. Rev. Lett.* **62**, 2644.
- Hart, M., Siddons, D. P. & Stajanoff, V. (1991). Private communication (see McWhan *et al.*, 1992).
- Hill, J. P., Feng, Q., Birgeneau, R. J. & Thurston, T. R. (1993). *Phys. Rev. Lett.* **70**, 3655–3658.
- Idzerda, Y. U., Tjeng, L. H., Lin, H.-J., Gutierrez, C. J., Meigs, G. & Chen, C. T. (1993). *Phys. Rev. B*, **48**, 4144–4147.
- Isaacs, E. D., McWhan, D. B., Kleiman, R. N., Bishop, D. J., Ice, G. E., Zschak, P., Gaulin, B. D., Mason, T. E., Garrett, J. D. & Buyers, W. J. L. (1990). *Phys. Rev. Lett.* **65**, 3185–3188.
- Jackson, J. D. (1975). *Classical Electrodynamics*, p. 453. New York: Wiley.
- Kakizaki, A., Fujii, J., Shimada, K., Kamata, A., Ono, K., Park, K.-H., Kinoshita, T., Ishii, T. & Fukutani, H. (1994). *Phys. Rev. Lett.* **72**, 2781–2784.
- Kao, C., Chen, C. T., Johnson, E. D., Hastings, J. B., Lin, H. J., Ho, G. H., Meiga, G., Brot, J.-M. & Hulbert, S. L. (1994). *Phys. Rev. B*. In the press.
- Kao, C., Hastings, J. B., Johnston, E. D., Siddons, D. P., Smith, G. C. & Prinz, G. A. (1990). *Phys. Rev. Lett.* **65**, 373–376.
- Keating, D. T. (1969). *Phys. Rev.* **178**, 732–742.
- Kisker, E., Schröder, K., Campagna, M. & Gudat, W. (1984). *Phys. Rev. Lett.* **52**, 2285–2288.
- Langridge, S., Stirling, W. G., Lander, G. H., Rebizant, J., Spirlet, J. C., Gibbs, D. & Vogt, O. (1994). *Europhys. Lett.* **25**, 137–142.
- Lovesey, S. W. (1993). *Rep. Prog. Phys.* pp. 257–326.
- Luo, J., Trammell, G. T. & Hannon, J. P. (1993). *Phys. Rev. Lett.* **71**, 287–290.
- Mackintosh, A. R. & Jensen, J. (1991). *Disorder in Condensed Matter Physics*, edited by J. A. Blackman & J. Taguena, p. 214. Oxford Univ. Press.
- McWhan, D. B., Hastings, J. B., Kao, C.-C. & Siddons, D. (1992). *Rev. Sci. Instrum.* **63**, 1404–1408.
- McWhan, D. B., Isaacs, E. D., Carra, P., Shapiro, S. M., Thole, B. T. & Hoshino, S. (1993). *Phys. Rev.* **47**, 8630–8633.
- McWhan, D. B., Vettier, C., Isaacs, E. D., Ice, G. E., Siddons, D. P., Hastings, J. B., Peters, C. & Vogt, O. (1990). *Phys. Rev.* **42**, 6007–6017.
- Majkrzak, C. F., Cable, J. W., Kwo, J., Hong, M., McWhan, D. B., Yafet, Y., Waszczak, J. V. & Vettier, C. (1986). *Phys. Rev. Lett.* **56**, 2700–2703.
- Maruyama, H., Iwazumi, T., Kawata, H., Koizume, Z., Fujita, M., Sakurai, H., Itoh, F., Namikawa, K., Yamazaki, H. & Ando, M. (1991). *J. Phys. Soc. Jpn.* **60**, 1456–1459.
- Moon, R. M. (1964). *Phys. Rev. A*, **136**, 195–202.
- Mulhollan, G. A., Andrews, A. B. & Erskine, J. L. (1992). *Phys. Rev. B*, **46**, 11212–11215.
- Namikawa, K., Ando, M., Nakajima, T. & Kawata, H. (1985). *J. Phys. Soc. Jpn.* **54**, 4099–4102.
- Platzman, P. M. & Tzoar, N. (1970). *Phys. Rev. B*, **2**, 3556–3559.
- Reck, R. A. & Fry, D. L. (1969). *Phys. Rev.* **184**, 492–495.
- Roth, Ch., Hillebrecht, F. U., Rose, H. B. & Kisker, E. (1993). *Phys. Rev. Lett.* **70**, 3479–3482.
- Samant, M. G., Stöhr, J., Parkin, S. S. P., Held, G. A., Hermsmeier, B. D. & Herman, F. (1994). *Phys. Rev. Lett.* **71**, 1112–1115.
- Schütz, G., Stähler, S., Knülle, M. & Fischer, P. (1993). *J. Appl. Phys.* **73**, 6430–6432.
- Schütz, G., Wagner, W., Wilhelm, W., Kienle, P., Zeller, R., Frahm, R. & Materlik, G. (1987). *Phys. Rev. Lett.* **58**, 737–740.
- Scott, G. G. & Sturmer, H. W. (1969). *Phys. Rev.* **184**, 490–491.
- Söderlind, P., Eriksson, O., Johansson, B., Albers, R. C. & Boring, A. M. (1992). *Phys. Rev. B*, **45**, 12911–12916.
- Stöhr, J., Wu, Y., Hermseier, B. D., Samant, M. G., Harp, G. R., Koranda, S., Dunham, D. & Tonner, B. P. (1993). *Science*, **259**, 658–661.
- Thole, B. T., Carra, P., Sette, F. & van der Laan, G. (1992). *Phys. Rev. Lett.* **68**, 1243–1246.
- Thurston, T. R., Helgesen, G., Gibbs, D., Hill, J. P., Gaulin, B. D. & Shirane, G. (1993). *Phys. Rev. Lett.* **70**, 3151–3154.
- Tonnerre, J. M., Jergel, M., Raoux, D., Idir, M., Soullier, G., Barchewitz, R. & Rodmacq, B. (1993). *J. Magn. Magn. Mater.* **121**, 230–233.
- Vettier, C. (1994). *J. Magn. Magn. Mater.* **129**, 59–65.
- Vettier, C., McWhan, D. B., Gyorgy, E. M., Kwo, J., Buntschuh, B. M. & Batterman, B. W. (1986). *Phys. Rev. Lett.* **56**, 757–760.
- Wu, R., Wang, D. & Freeman, A. J. (1993). *Phys. Rev. Lett.* **71**, 3581–3584.
- Wu, Y., Stöhr, J., Hermsmeier, B. D., Samant, M. G. & Weller, D. (1992). *Phys. Rev. Lett.* **69**, 2307–2310.
- Yafet, Y. (1987). *J. Appl. Phys.* **61**, 4058–4060.